Acta Pharmaceutica Sinica B 2021;11(5):1213−1226

Chinese Pharmaceutical Association
Institute of Materia Medica, Chinese Academy of Medical Sciences

Acta Pharmaceutica Sinica B

www.elsevier.com/locate/apsb
www.sciencedirect.com

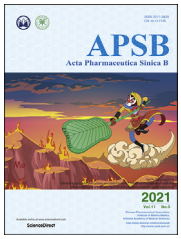

ORIGINAL ARTICLE

Gut microbiota mediates the absorption of FLZ, a new drug for Parkinson's disease treatment

Junmei Shang[†], **Shurong Ma**[†], **Caixia Zang**, **Xiuqi Bao**[*], **Yan Wang**[*], **Dan Zhang**[*]

Department of Pharmacology, Institute of Materia Medica, Chinese Academy of Medical Sciences and Peking Union Medical College, Beijing 100050, China

Received 9 August 2020; received in revised form 4 October 2020; accepted 3 November 2020

KEY WORDS

FLZ;
Parkinson's disease;
Gut microbiota;
CYP51;
COMT

Abstract The gut microbiota plays an important role in regulating the pharmacokinetics and pharmacodynamics of many drugs. FLZ, a novel squamosamide derivative, has been shown to have neuroprotective effects on experimental Parkinson's disease (PD) models. FLZ is under phase I clinical trial now, while the underlying mechanisms contributing to the absorption of FLZ are still not fully elucidated. Due to the main metabolite of FLZ was abundant in feces but rare in urine and bile of mice, we focused on the gut microbiota to address how FLZ was metabolized and absorbed. *In vitro* studies revealed that FLZ could be exclusively metabolized to its major metabolite M1 by the lanosterol 14 alpha-demethylase (CYP51) in the gut microbiota, but was almost not metabolized by any other metabolism-related organs, such as liver, kidney, and small intestine. M1 was quickly absorbed into the blood and then remethylated to FLZ by catechol *O*-methyltransferase (COMT). Notably, dysbacteriosis reduced the therapeutic efficacy of FLZ on the PD mouse model by inhibiting its absorption. The results show that the gut microbiota mediate the absorption of FLZ through a FLZ−M1−FLZ circulation. Our research elucidates the vital role of the gut microbiota in the absorption of FLZ and provides a theoretical basis for clinical pharmacokinetic studies and clinical application of FLZ in the treatment of PD.

© 2021 Chinese Pharmaceutical Association and Institute of Materia Medica, Chinese Academy of Medical Sciences. Production and hosting by Elsevier B.V. This is an open access article under the CC BY-NC-ND license (http://creativecommons.org/licenses/by-nc-nd/4.0/).

*Corresponding authors. Tel./fax: +86 10 63165203.
E-mail addresses: danzhang@imm.ac.cn (Dan Zhang), wangyan@imm.ac.cn (Yan Wang), baoxiuqi@imm.ac.cn (Xiuqi Bao).
[†]These authors made equal contributions to this work.
Peer review under responsibility of Chinese Pharmaceutical Association and Institute of Materia Medica, Chinese Academy of Medical Sciences.

https://doi.org/10.1016/j.apsb.2021.01.009
2211-3835 © 2021 Chinese Pharmaceutical Association and Institute of Materia Medica, Chinese Academy of Medical Sciences. Production and hosting by Elsevier B.V. This is an open access article under the CC BY-NC-ND license (http://creativecommons.org/licenses/by-nc-nd/4.0/).

1. Introduction

The human gastrointestinal tract harbors a complex and dynamic population of gut microbiota, consisting of at least 10^{14} bacteria and archaea with a total amount of 10 times that of the human body[1]. It is considered to be an indispensable "metabolic organ" that provides the body with a variety of enzymes and biochemical metabolic pathways[2,3]. The gut microbiota plays critical roles in maintaining human health by regulating metabolism, immunity, and nerves; therefore, the disturbance of the gut microbiota leads to the occurrence and development of various diseases, such as inflammatory bowel disease[4], cardiovascular disease[5], liver disease[6], and neurodegenerative disease[7].

Increasing evidences have shown that gut microbiota is also involved in drug metabolism by affecting their structures and activities. Through studying the metabolisms of 271 drugs by 76 human gut microbiota, researchers have found that many drugs are chemically modified by microbes[8]. The bioavailability of orally administered drugs depends on the extent of the first-pass metabolism by intestinal and hepatic enzymes prior to reaching the systemic circulation. In fact, a variety of enzymes are found in the gut microbiota, which can interact with drugs and generate metabolites that differ from those in other host organs, promoting drug absorption and influencing therapeutic outcome[9–11]. For example, azoreductase of the gut microbiota catalyzes the azoreduction of drugs, including prontosil, neoprontosil, and sulfasalazine, activating azo-bond containing pro-drug[12–15]. Therefore, the research for discovering the role of gut microbiota in the pharmacokinetics and therapeutic characteristics of drugs is significant.

FLZ, formulated as *N*-2-[(4-hydroxyphenyl)-ethyl]-2-(2,5-dimethoxy-phenyl)-3-(3-methoxy-4-hydroxyphenyl)-acrylamide, is a novel synthetic derivative of squamosamide and the application on Parkinson's disease (PD) is going through the phase I clinical trial now. Our previous studies demonstrated that FLZ could cross the blood–brain barrier (BBB) and has strong neuroprotective effects on several experimental PD models[16–18]. However, the current underlying mechanisms for metabolism and absorption of FLZ are still not fully elucidated. Our previous study demonstrated that M1, the main demethylated metabolite of FLZ, formulated as *N*-2-[(4-hydroxyphenyl)-ethyl]-2-(2,5-dimethoxy-phenyl)-3-(3,4-dihydroxy-phenyl)-acrylamide, was abundant in feces but rare in urine and bile of mice (unpublished data), leading us to speculate whether the gut microbiota was involved in FLZ metabolism. Therefore, in the present study, we designed a set of experiments to investigate whether and how the gut microbiota affected the profiles of metabolism, absorption, and neuroprotective efficacy of FLZ both *in vitro* and *in vivo*. The results show that the vast majority of FLZ was demethylated to M1 in the gut microbiota, and then M1 was soon absorbed into the blood, where M1 was remethylated to FLZ. Lanosterol 14 alpha-demethylase (CYP51) in gut microbiota and catechol *O*-methyltransferase (COMT) in blood mainly participate in this transformation. The gut microbiota mediated the absorption of FLZ through FLZ–M1–FLZ circulation and accordingly, further regulated the therapeutic effects of FLZ on PD. The process provided a paradigm showing the ways that gut microbiota participates in FLZ metabolism and absorption, suggesting the importance of gut microbiota in modifying the bioavailability and therapeutic efficacy of FLZ.

2. Materials and methods

2.1. Animals

Male C57BL/6 mice (22–25 g) and KM mice (22–25 g) were supplied by the Institute of Laboratory Animal Science, Chinese Academy Medical Sciences (Beijing, China). The animals were maintained in a 12 h light/dark cycle at a temperature of 22–24 °C in a relative humidity of 60% room, and received food and water *ad libitum*. Animals were adapted for 1 week to the conditions described above before experimentation. All experimental procedures were performed in accordance with the guidelines of the Beijing Municipal Ethics Committee for the Care and Use of Laboratory Animals.

2.2. Qualitative analysis of FLZ and its metabolites by LC/MS^n-IT-TOF in colonic contents

FLZ and M1 with the purity >99%, synthesized by the Department of Medicinal Chemistry, Institute of Materia Medica, Chinese Academy of Medical Sciences (Beijing, China), were incubated with the gut microbiota. The method for the preparation of the gut microbiota was previously described[11]. Briefly, colonic contents from mice were pooled, and 4 g of the sample was transferred to a flask containing the anaerobic medium (Solarbio Science & Technology, Beijing, China). After thoroughly mixed and filtrated, the cultures were pre-incubated under anaerobic conditions with N_2 atmosphere at 37 °C for 30 min. Then FLZ (5 mmol/L) was incubated with the gut microbiota for 48 h with dimethyl sulfoxide as the negative control. After termination of the reaction with 3-fold of acetonitrile and centrifugation at 14,000 rpm (2K15, Sigma, St. Louis, MO, USA) for 5 min, the supernatant was dried under nitrogen flow at room temperature, and the residue was dissolved in 100 μL of acetonitrile:water (*v*/*v*) = 1:1. Then 10 μL supernatant was injected for analysis after centrifugation. A liquid chromatography instrument coupled to an ion trap time-of-flight mass spectrometer (LC/MS^n-IT-TOF) from Shimadzu Corporation (Kyoto, Japan) was used to identify the chemical structures of FLZ and its possible metabolites.

2.3. Quantitative analysis of FLZ and M1 by LC–MS/MS

Liquid chromatography with tandem mass spectrometry (LC–MS/MS 8050, Shimadzu Corporation) was used for the quantification of FLZ and M1 in biological samples. LC separation was achieved by an XSelect HSS T3 column (100 mm × 2.1 mm × 3.5 μm, Waters, Milford, MA, USA) with a 0.3 mL/min flow rate at 30 °C. The mobile phase was combined by acetic acid:water (phase A, 0.3:100, *v*/*v*) and acetonitrile (phase B), and a binary isocratic elution (A:B = 60:40, *v*/*v*) was performed for 7 min. Multiple reaction monitoring (MRM) modes were used during the analysis: 449.95→313.15 for FLZ, 436.25→299.15 for M1, and 236.85→194.15 for IS. The mass parameters were set as the following: nebulizer gas, 2.9 L/min; drying gas, 10.0 L/min; heating gas, 10.0 L/min; interface voltage, −4.5 kV; interface temperature: 250 °C; CID gas, 230 kPa; DL temperature and heat block temperature: 250 and 300 °C, respectively. The auto-sampler was kept at 4 °C. The cultured sample (100 μL) was mixed with 10 μL of the internal standard (carbamazepine, 400 ng/mL in methanol) and 90 μL distilled

water. After that, 1 mL ethyl acetate was added for extraction and 900 μL of the supernatant was dried. The residue was dissolved in 100 μL of acetonitrile:water (*v*/*v*) = 40:60, and 10 μL supernatant was injected for analysis after centrifugation. The concentrations for standard curve were: 0.1, 0.2, 0.5, 2, 10, 50, 200, 500, and 2000 ng/mL. Shimadzu LC−MS solution (version 5.72) was used for data acquisition and processing.

2.4. Quantitative analysis of FLZ and M1 in the gut microbiota and single bacterial strains

FLZ (0.2 mg/mL) was incubated with the prepared gut microbiota at 37 °C under anaerobic conditions for 4 h. The resulting cultures (100 μL) at different points (0, 15, 30, 60, 120, and 240 min) were immediately extracted as described above and dissolved in 100 μL of acetonitrile:water (*v*/*v*) = 40:60. The concentrations of FLZ and M1 in cultures were determined by LC−MS/MS. Fifteen single bacterial strains, including *Acinetobacter baumannii*, *Pseudomonas aeruginosa*, *Shigella boydii*, *Proteus mirabilis*, *Enterococcus faecalis*, *Enterococcus faecium*, *Proteus vulgaris*, *Enterobacter aerogenes*, *Staphylococcus epidermidis*, *Escherichia coli*, *Staphylococcus aureus*, *Enterobacter cloacae*, *Lactobacillus acidophilus*, *Lactobacillus casei* and *Bifidobacterium longum* (Nanjing Bianzhen Biotechnology Co., Ltd., Nanjing, China) were activated and amplified in the proper medium. The optical density (OD) was determined at 600 nm to unify the total number of 15 bacteria colonies at 3×10^8 CFU/mL. Then bacteria strains were respectively incubated with FLZ (0.2 mg/mL) at 37 °C for 12 h, and the levels of FLZ and M1 were detected by LC−MS/MS.

2.5. Quantitative analysis of FLZ and M1 in microsomes, S9, cytosol, intestine, and blood

For the preparation of S9, cytosol, and microsomes, the liver and kidney from mice were homogenized in Tris/KCl buffer (22 mL/g, pH 7.4). After centrifuged at 10,000×*g* for 25 min, S9 was isolated in the supernatant. And then Tris/KCl was added and centrifuged at 105,000×*g* for 1 h to obtain cytosol in the supernatant and microsomes in the precipitation. 200 μL of the culture system containing S9, cytosol, or microsomes (0.5 mg/mL protein), 2 μL of 0.2 mg/mL FLZ or M1, 0.05 mmol/L Tris/HCl (pH = 7.4) with or without 20 μL of NADPH system (1 mmol/L), was incubated at different points (0, 15, 30, 60, and 120 min). 100 μL of culture was determined by LC−MS/MS for analysis of FLZ and M1, respectively. The small intestine was collected and homogenized with 4-fold (*w*/*v*) phosphate buffer solution to obtain gut microsomes. The whole blood sample was treated with heparin after collected. And then the same amount of FLZ or M1 was added into the small intestine homogenate or blood, respectively, incubated and determined at different points (0, 15, 30, 60, and 120 min) as described above.

2.6. Quantification analysis of FLZ and M1 in mouse plasma and brain

KM mice were fasted for 12 h and then orally treated with FLZ or M1 (50 mg/kg). Blood samples were collected at 0, 0.25, 0.5, 0.75, 1, 1.25, 2, 3, 4, 6, 10, 24, and 48 h after treatment, centrifuged at 6000×*g* for 5 min, and then plasma was obtained for metabolite analysis. The brain samples were collected at 0, 0.5, 1, 2, 4, 6, and 10 h after administration. The method for brain preparation was conducted as previously described[19]. 10 μL supernatant of plasma or brain was injected into the LC−MS/MS for analysis of FLZ and M1.

2.7. Molecular docking

BIOVIA Discovery Studio Client software (version 2016; Accelrys, Inc., San Diego, CA, USA) was employed to perform the molecular docking of FLZ onto the lanosterol 14-alpha-demethylase (CYP51, https://doi.org/10.2210/pdb5ESE/pdb), and M1 onto the catechol *O*-methyltransferase (COMT, https://doi.org/10.2210/pdb4O0Q/pdb). The crystal structures of CYP51 and COMT are available in the Protein Data Bank. The CDOCKER mode was chosen as the binding algorithm of compounds with the enzymes. The docking parameters were set to the default values except that the pose cluster radius was set at 0.5. The grid boxes were the active site cavities. The binding results of compounds with the enzymes were expressed according to their binding free energy.

2.8. Inhibition of CYP51 in gut microbiota and COMT in the blood

To inhibit CYP51 in gut microbiota, two selective CYP51 inhibitors, itraconazole and voriconazole, were added to the colonic contents and incubated with FLZ, respectively. The reaction system of colonic contents contained FLZ (2 μg/mL) and itraconazole (8 and 20 μg/mL) or voriconazole (8 and 20 μg/mL) with the anaerobic medium in a final volume of 1 mL, and 100 μL of the resulting culture was performed for analysis. To inhibit COMT in blood, entacapone, the selective COMT inhibitor was added to the blood samples and incubated with M1. The 100 μL reaction system in the blood consisted of M1 (2 μg/mL), entacapone (2, 8, and 16 μg/mL) and the heparin-treated whole blood samples. After incubation, 3-fold volume of ice-cold acetonitrile was added to terminate the reactions in the colonic contents and blood, respectively, and then they were centrifuged at 14,000 rpm (2K15, Sigma) for 5 min. The supernatant was evaporated to dryness under a nitrogen flow and dissolved with an equal volume of the mobile phase for LC−MS/MS analysis of FLZ and M1.

2.9. Measurement the activities of CYP51 and COMT

The activity of CYP51 in *A. baumanii* and feces of mice was detected by microbial-derived ELISA kit (Shanghai Meilian Biotechnology Co., Ltd., Shanghai, China) according to the manufacturer's instructions. Briefly, samples, standards, and horseradish peroxidase (HRP)-labeled antibody were added into pre-coated microwells with CYP51 capture antibody. After incubation for 1 h, the substrate tetramethyl benzidine (TMB) was added and the OD value was measured at 450 nm to calculate the CYP51 concentration of the samples.

Activities of CYP51 in colonic contents and COMT in blood were monitored by substrate catalyze reactions. For CYP51 activity assay in colonic contents, the substrate of microbial CYP51, 0.05 mmol/L lanosterol, was added into the reaction system of colonic contents containing FLZ and itraconazole or voriconazole. After incubation for 6 h, 100 μL of the resulting solution was mixed with 300 μL of methanol. The supernatant was dried under

N_2 atmosphere after centrifugation, and then 100 μL of acetonitrile and 100 μL of bis-(trimethylsilyl)-trifluoroacetamide (TCIsy Development Co., Ltd., Shanghai, China) were added. After derivatization at 70 °C for 1 h (in darkness), the demethylated metabolite (14-demethyl-lanosterol, *m/z* 483, 379) in the resulting solution was analyzed by GC−MS QP 2010 (Shimadzu, Japan). In detection of COMT activity in mouse blood, 0.05 mmol/L 3,4-hydroxybenzoic acid, the substrate of COMT, was mixed with the blood samples. After incubation with entacapone for 2 h, the 4-fold volume of cold acetonitrile was added to terminate the reaction. And then the produced 4-hydroxy-3-methoxybenzoicacid in the supernatant was detected by LC−MS/MS 8050 (Shimadzu, Japan) using the positive MRM mode (*m/z* 168.30 → 108.55 for 4-hydroxy-3-methoxybenzoicacid).

2.10. Development of PD mouse model, pseudo-germ-free (PGF) mouse model and treatments

C57/BL mice were intraperitoneally injected with probenecid (250 mg/kg in DMSO, Sigma, MO, USA) 30 min prior to subcutaneously injection of MPTP hydrochloride (25 mg/kg in saline, Sigma) to induce parkinsonian symptoms. These mice have received a total of 10 injections of MPTP in combination with probenecid (MPTP/p). The 10 injections were given at an interval of 3.5 days for a 5-week schedule.

For the preparation of PGF mice, normal C57/BL mice and MPTP/p mice were orally treated with a broad-spectrum antibiotic cocktail, including cefadroxil 100 mg/kg, terramycin 300 mg/kg, and erythromycin 300 mg/kg (Solarbio Science & Technology), twice a day for 3 days. The colonic contents of the mice were collected on the third day to confirm the PGF status by culturing fecal samples aerobically on a nutrient agar culture medium. Colonic contents from normal C57/BL mice and MPTP/p mice served as control. The normal C57/BL mice, antibiotic-exposed normal mice, MPTP/p mice, and antibiotic-exposed MPTP/p mice were then treated with FLZ (75 mg/kg) once a day for 8 weeks. Meanwhile, the antibiotic-exposed normal mice and antibiotic-exposed MPTP/p mice were continuing to treat with the same dose of antibiotic cocktail once a day for 8 weeks to maintain the pseudo-sterile state. 24 h after the last administration, blood and brains of mice were collected, and feces of mice were collected within 24 h of the last administration to detect the concentrations of FLZ and M1. Mouse brain was collected to detect the pathological related markers of PD.

2.11. Rotarod test

The rotarod test, which requires animals to balance and walk on a rotating cylinder, is a widely used test to measure coordinated motor skills that have also been employed in the MPTP/p mouse model. Mice were positioned on the rotarod and then tested on the revolving rod at the speed of 25 rpm for up to 120 s. The rotarod automatically recorded the time that the animals first fell off the rod, which designated as latency. Animals were pre-trained three times before MPTP/p lesion until more or less ceiling performance was reached. On the post-MPTP/p testing day, mice were tested twice, and the time of latency was recorded. Between each trial, animals rested for 1 h. The behavioral test of the normal control mice, MPTP/p mice, MPTP/p mice treated with FLZ, and antibiotic-exposed MPTP/p mice treated with FLZ were performed at 13th week (the last day of FLZ administration).

2.12. Immunohistochemical analysis

Mice were anesthetized with pentobarbital and perfused transcardially with saline and then with cold 4% paraformaldehyde in 0.1 mol/L phosphate buffer (pH 7.4). Brains were then removed and sectioned to 40-μm sections at the same position. Coronal sections through the substantia nigra were processed for tyrosine kinase (TH) immunohistochemistry as previously described[20]. Briefly, sections were incubated with rabbit polyclonal TH antibody (1:500, Abcam, CA, USA) and then incubated with the biotinylated secondary antibody and subsequently with avidin-peroxidase. Finally, the labeling was visualized with 0.05% 3,3′-diaminobenzidine (DAB). Four consecutive sections of each mouse were selected to observe TH-positive neurons in the substantia nigra with light microscopy (Nikon E600, Japan), and the total number of positively stained cells in each group was calculated. All evaluations were done by a researcher blind to the experiment.

2.13. Quantitative real-time PCR (qPCR)

The gene expression levels of *Il-6*, *Il-1β*, *Iba-1*, *Cox-2*, and *Il-10* were quantified by real-time PCR analysis. Briefly, RNA of mice midbrain was extracted by Trizol reagent according to the manufacturer's instructions. Reverse transcription kit (Thermo) was used to transcribe RNA to cDNA. After that, the qPCR was conducted using the SYBR Green Real-time PCR Master Mix according to the manufacturer's protocols. Primer sequences are listed for qPCR analysis in Table 1. Cycling parameters of qPCR reaction were 94 °C for 5 min, followed by 32 cycles of 94 °C for 30 s, 59 °C for 30 s, and 72 °C for 60 s with a final extension at 72 °C for 7 min. All samples were run in triplicate, and the relative gene expression was calculated using the $2^{-\Delta\Delta Ct}$ method. Cycle time values of the genes were first normalized with β-actin of the same samples, and then the relative differences between the control and treatment groups were calculated and expressed as relative increases, where the control was set at 100%.

2.14. Detection of dopamine and its metabolites in the striatum of mice

The striatum of mice in each group was collected on ice and homogenate in saline at 1:10 (*w/v*). 50 μL of the mixture was added with 200 μL of acetonitrile as the internal standard. After

Table 1 Primers used for qPCR.

Gene	Primer sequence
Il-6	Forward: CTGCAAGAGACTTCCATCCAG
	Reverse: AGTGGTATAGACAGGTCTGTTGG
Il-1β	Forward: GCTACCTATGTCTTGCCCGT
	Reverse: GACCATTGCTGTTTCCTAGG
Iba-1	Forward: ATCAACAAGCAATTCCTCGATGA
	Reverse: CAGCATTCGCTTCAAGGACATA
Cox-2	Forward: GAAGTGGGGGTTTAGGATCATC
	Reverse: CCTTTCACTTTCGGATAACCA
Il-10	Forward: GAATTCCCTGGGAGAGAAGC
	Reverse: TTCTCACAGGGGAGAAATCG
β-Actin	Forward: AGAAGCTGTGCTATGTTGCTCTA
	Reverse: TCAGGCAGCTCATAGCTCTTC

centrifugation, the supernatant was dried under N_2 atmosphere and redissolved in 50 μL acetonitrile:water (5:95, *v*/*v*). After centrifugation again, 5 μL supernatant was pipetted for the analysis of dopamine (DA), dihydroxyphenylacetic acid (DOPAC), and homovanillic acid (HVA). The neurotransmitters for determination were separated by a C18 column (100 mm × 5 mm × 3 μm), and the mobile phase consisted of 0.05% formic acid−water (phase A) and acetonitrile (phase B). Gradient elution conditions were as following (A:B, *v*/*v*): 0.01 min: 95:5; 1.01 min: 70:30; 5.00 min: 5:95; 6.00 min: 5:95; 7.01 min: 5:95; 10.00 min; controller stop. The C18 column was maintained at 30 °C and flow rate was 0.5 mL/min. Both positive and negative MRM modes were used for quantification: 154.20→91.10 for DA (+), 167.10→123.10 for DOPAC (−), and 182.20→83.10 for HVA (−). Other mass parameters were set as following: nebulizer gas, 2.7 L/min; drying gas, 10.0 L/min; heating gas, 10.0 L/min; interface voltage, −4.5 kV; interface temperature, 300 °C; CID gas, 230 kPa; DL temperature and heat block temperature, 250 and 300 °C, respectively. The levels of dopamine and its metabolites in the striatum of PD model were evaluated by LC−MS/MS 8050 (Shimadzu).

2.15. Western blot assay

The midbrain of the mice was lysed using non-denaturing lysis buffer, and immunoblotting was performed as previously described[21]. Protein homogenates were subjected to Western blot analysis using antibodies against CD68, GFAP, and GAPDH (ABclonal, Wuhan, China). The blots were visualized by incubating the membranes with ECL Plus reagents (Yeasen, Shanghai, China) and developed with a LAS 4000 chemiluminescence system (Fujifilm, Tokyo, Japan). The densities of the bands were determined using Gel-Pro Analyzer 4.0 software (Media Cybernetics, MD, USA).

2.16. Statistical analysis

Statistical analysis was performed with SPSS 18.0 statistical software (SPSS Inc., Chicago, IL, USA). Data are expressed as mean ± standard deviation (SD). The significant differences among groups were determined with One-way ANOVA followed by LSD *t*-test. $P < 0.05$ was considered as statistical significance.

3. Results

3.1. M1 was the main metabolite of FLZ generated by the gut microbiota

We have previously detected eight metabolites of FLZ in experimental animals, among which M1, the demethylated product of FLZ, was the main metabolite in quantity. Since M1 was abundant in feces, we speculated that the gut microbiota might be involved in the conversion of FLZ to M1. To verify this hypothesis, we incubated FLZ with mouse colonic contents to identify the possible metabolites of FLZ and their chemical structures. In the culture of the colonic contents and FLZ, both FLZ (t_R = 13.8 min) and M1 (t_R = 12.2 min) were detected, indicating that FLZ could be converted to M1 by the gut microbiota (Fig. 1A). The extracted ion chromatograms (EICs) obtained from LC/MS^n-IT-TOF analysis show that FLZ and M1 were responded well in the positive ion analysis mode (FLZ: 450.1532, M1: 436.1430, Fig. 1B). We then elucidated the profiles of FLZ conversion to M1 (Fig. 1C). Incubation of FLZ (0.2 mg/mL) with the colonic contents of mice resulted in a gradually decreased level of FLZ, and accordingly, M1 was detectable within 15 min of incubation. The absolute quantification results showed that almost all FLZ was transformed to M1 after incubation in the colonic contents for 60 min, and the generated M1 was at a stable level within 60−240 min, indicating that during this period, M1 was not metabolized by the gut microbiota (Fig. 1D). To further determine gut microbiota is responsible for the FLZ-to-M1 conversion, we incubated FLZ (50 μg/mL) with the 15 gut microbiota strains *in vitro*, and then detected the concentrations of M1 and FLZ in the cultures, respectively. As shown in Fig. 1E, among the 15 gut microbiota strains, *A. baumanii*, *P. aeruginosa*, *S. boydii*, *P. mirabilis*, *E. faecalis* and *E. faecium* metalized FLZ to M1 after 12 h-incubation. It was worth noting that the ratio of M1/FLZ in *A. baumanii* was higher compared with all the other investigated bacteria (Fig. 1E). These data suggest that M1 was the main metabolite of FLZ which was converted by gut microbiota.

3.2. The liver, kidney, and small intestine were not the main organs in the conversion of FLZ to M1

To determine whether the gut microbiota is specific and mainly responsible for FLZ-to-M1 conversion, we incubated FLZ (0.2 mg/mL) or M1 (0.2 mg/mL) with different metabolic components that were rich in drug metabolic enzymes, including the microsomes, S9, cytosol of the liver and kidney, as well as the microsomes of the small intestine, and then measured the amounts of FLZ and M1 in the cultures. As shown in Fig. 2A, after incubating for 30 min, FLZ can be metabolized in the liver microsomes system, while a very low concentration of M1 was detected in the culture, and M1 was not detected in the system of liver S9 or liver cytosol. To further confirm the role of NADPH in FLZ conversion, we incubated FLZ with NADPH and non-NADPH system for 120 min in liver microsomes. The result shows that the transformation of FLZ to M1 was a NADPH dependent enzymatic reaction (Fig. 2B). Besides, FLZ was not detected when M1 was incubated with liver microsomes, S9, and cytosol (Fig. 2C and D). These results reveal that both FLZ and M1 could be metabolized in the liver S9 and microsomes system, but nearly no mutual conversion between FLZ and M1. When FLZ or M1 was incubated with microsomes, S9, cytosol of the kidney, there was almost no M1 or FLZ detected, suggesting that there was nearly no conversion between FLZ and M1 in the kidney (Fig. 2E and F). In addition, FLZ could be metabolized by small intestine microsomes with no M1 detected (Fig. 2G), while M1 was almost not metabolized by small intestine microsomes (Fig. 2H), indicating that M1 was not a metabolite of FLZ in small intestine microsomes. These results exclude the role of liver, kidney, and small intestine in the metabolism of FLZ to M1, and indirectly confirmed the uniqueness of the gut microbiota in FLZ-to-M1 conversion.

3.3. CYP51 was involved in the conversion of FLZ to M1 in the gut microbiota

We further explored the enzyme involved in the conversion of FLZ to M1 in the gut microbiota. CYP51 is the most abundant demethylase in the gut microbiota[22], and a high level of CYP51 activity was found in *A. baumanii*, the main bacterium that metabolized FLZ to M1 in the present study (Supporting

Information Fig. S1). We then performed computer-assistant virtual docking by BIOVIA Discovery Studio Client software to study the binding activity of CYP51 to FLZ. The result shows that FLZ exhibited excellent docking performance on CYP51, with a binding free energy of −56.0122 kcal/mol (Fig. 3A and B). FLZ could possibly anchor into the binding site of CYP51 with the following interactions: the hydrogen bond between the phenolic hydroxyl group and the site of His225, Lys351, Arg469; the carbon−hydrogen bond between the oxygen of another phenolic hydroxyl group and Gly464; and the pi−alkyl interaction between the benzene ring and Cys479, Leu380.

To further clarify whether CYP51 is a key enzyme that mediates the demethylation of FLZ, inhibitors of CYP51, itraconazole and voriconazole, were employed to further validate the speculation. As shown in Fig. 3C, the activity of CYP51 in the reaction system of colonic contents was inhibited by itraconazole and voriconazole in a dose-dependent manner, respectively. Accordingly, the concentration of FLZ was increased and M1 was decreased in the colonic contents (Supporting Information Fig. S2), and therefore reduced the ratio of M1/FLZ (Fig. 3D). These data suggest that the activity of CYP51 in gut microbiota was positively correlated with the capability of metabolizing FLZ, supporting our finding that CYP51 might be the key enzyme in the conversion of FLZ to M1.

3.4. Pharmacokinetics study of FLZ and M1 in plasma and brain of mice

The pharmacokinetic profiles of FLZ and M1 are represented in Fig. 4. After the oral administration of FLZ, there was a bimodal phenomenon of the concentration−time curve of FLZ in plasma. The peak time was 5 and 180 min, respectively, and the C_{max} was about 361.0 ng/mL with rapid elimination in plasma (Fig. 4A). However, incubated with FLZ in plasma, the concentration of M1 was only about 1−2 ng/mL (Fig. 4B), therefore resulted in relatively a low ratio of M1/FLZ in mouse plasma treated with FLZ (Fig. 4C). When oral administration of mice with an equal dosage of M1, FLZ was soon detected and the concentration reached its peak at 2 h, with C_{max} about 259.8 ng/mL, while the concentration of M1 in the plasma was only about 1−2 ng/mL (Fig. 4D and E).

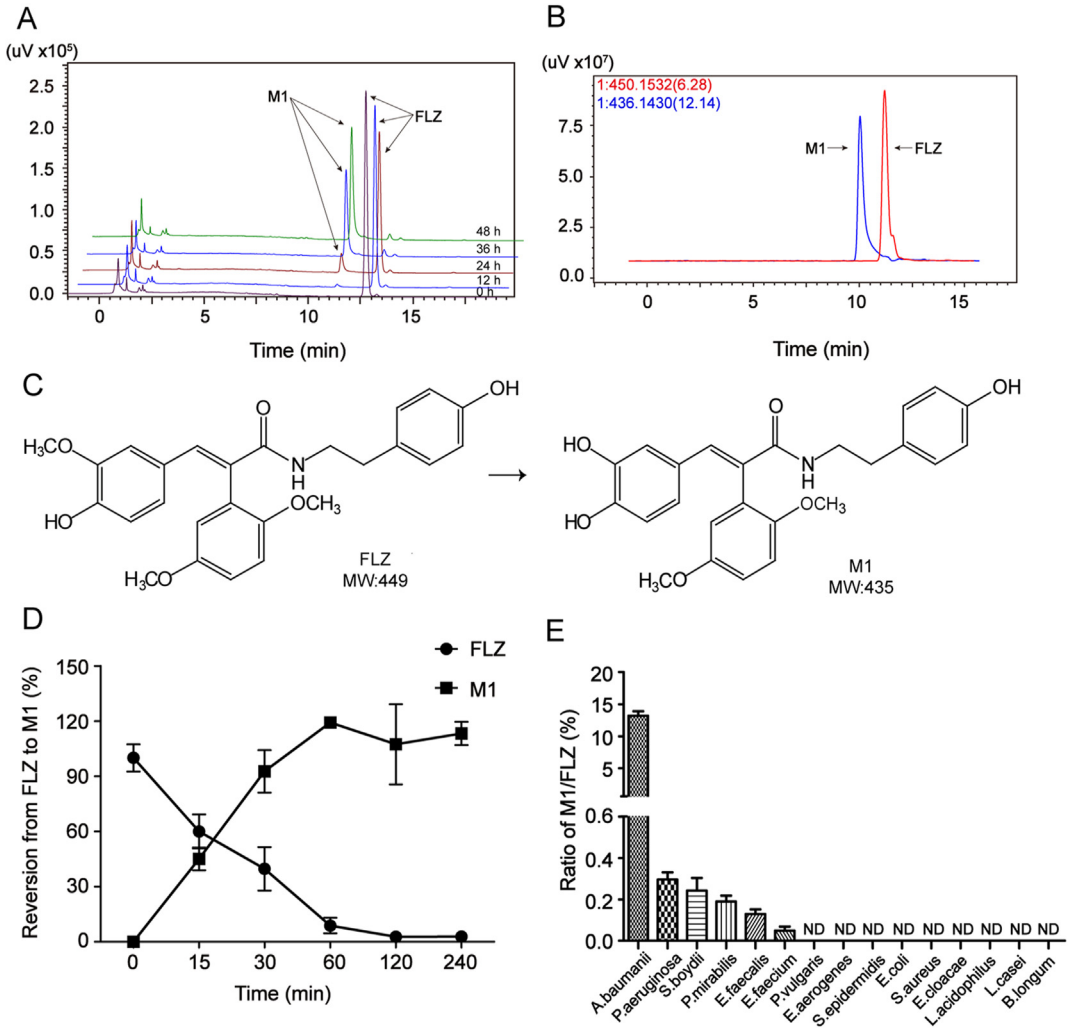

Figure 1 FLZ is metabolized to M1 by the gut microbiota. (A) HPLC chromatogram of FLZ-to-M1 conversion in mice colonic contents (FLZ: t_R = 13.8 min, M1: t_R = 12.2 min). (B) EIC of M1 and FLZ in positive ion mode, the *m/z* values in this chromatogram: M1, 436; FLZ, 450. (C) The molecular formula and metabolic process of FLZ to M1. (D) Conversion of FLZ to M1 by the gut microbiota in colonic contents (n = 4 in each group). (E) The ratio of M1/FLZ in 15 intestinal bacteria strains (n = 6 in each group). Data are presented as mean ± SD, n = 4.

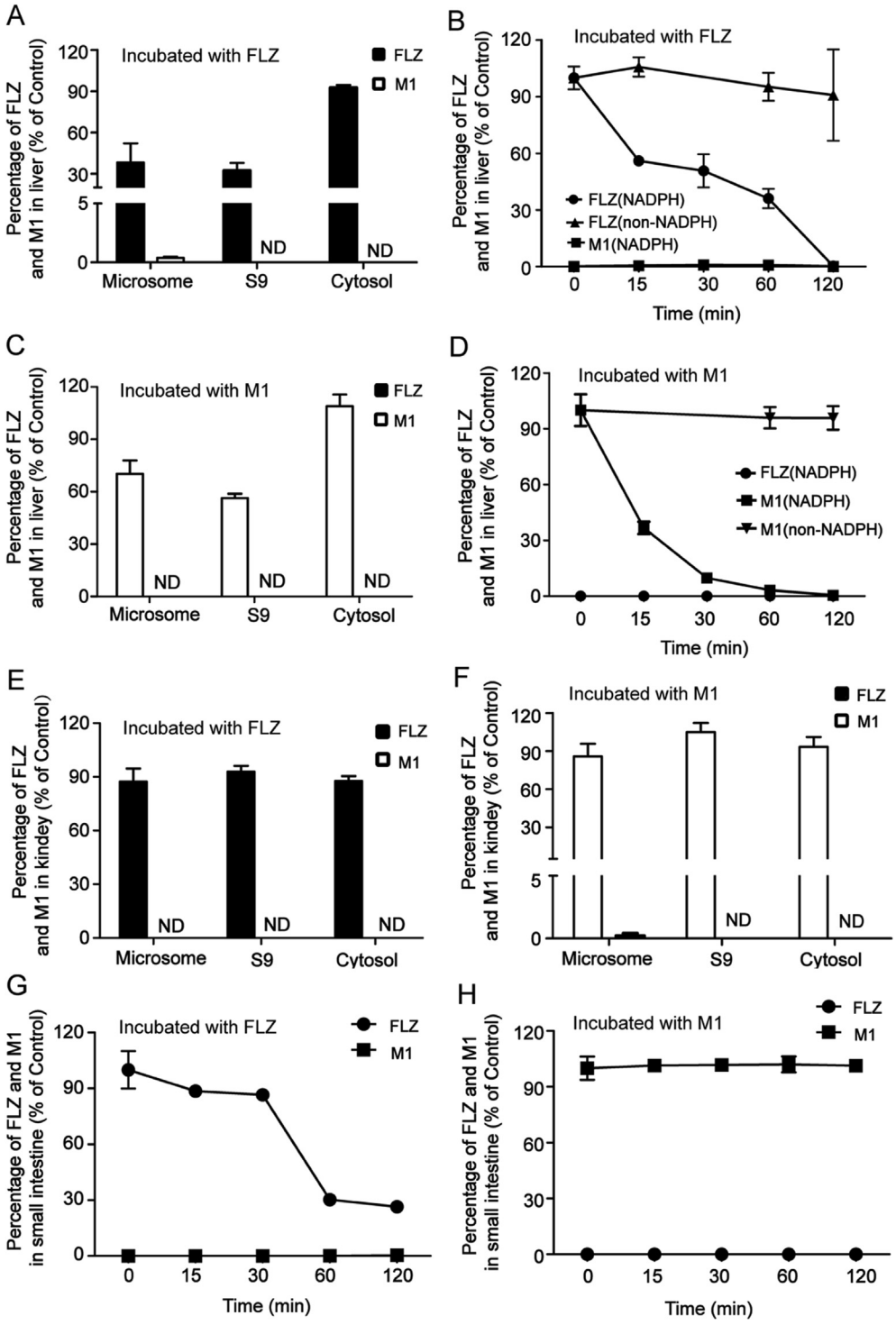

Figure 2 The metabolism of FLZ and M1 in liver, kidney, and small intestine. Microsomes, S9, and cytosol of liver and kidney as well as small intestine were extracted from mice and then incubated with FLZ or M1. Percentage of FLZ and M1 in mouse liver microsomes, S9, and cytosol incubated with FLZ (A) or M1 (C) at 30 min. Percentage of FLZ and M1 in mouse liver microsomes incubated with FLZ (B) or M1 (D) for 120 min. Percentage of FLZ and M1 in mouse kidney microsomes, S9, and cytosol incubated with FLZ (E) or M1 (F) at 30 min. Percentage of FLZ and M1 in mouse small intestine homogenate incubated with FLZ (G) or M1 (H) for 120 min. Data are presented as mean ± SD ($n = 4$ in each group). ND: not detected.

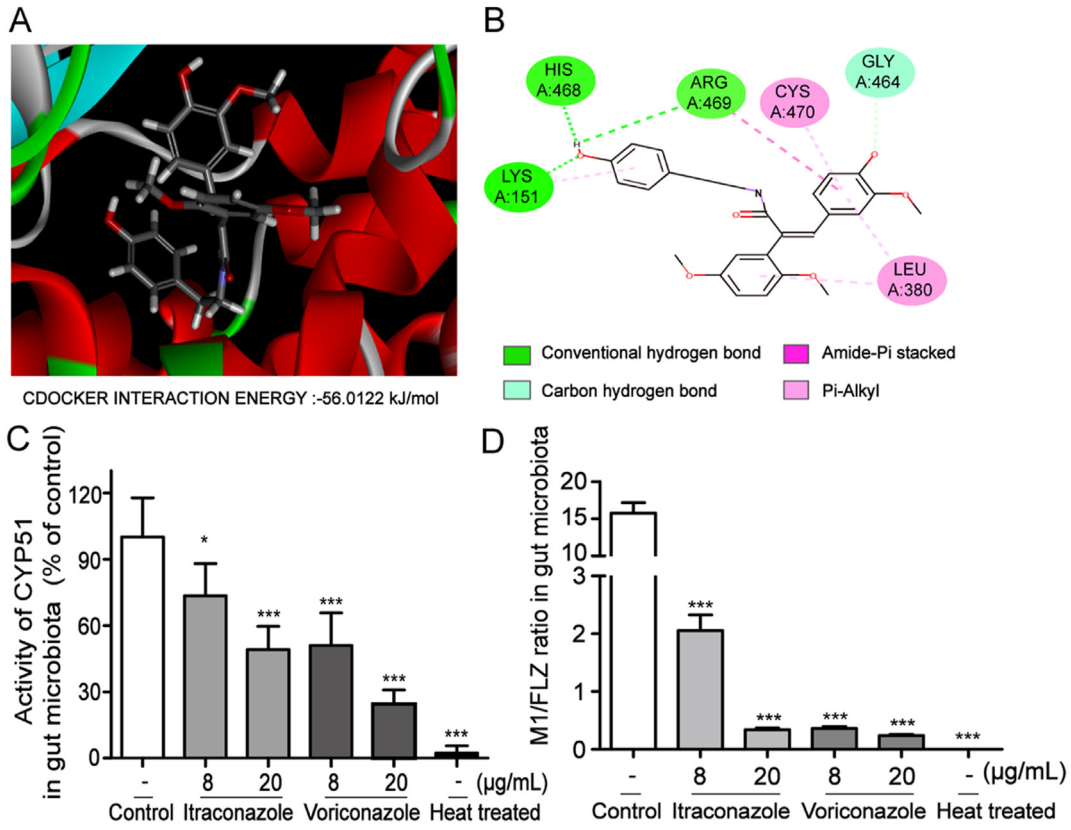

Figure 3 CYP51 contributed to the conversion of FLZ to M1 in the gut microbiota. Molecular docking was performed by BIOVIA Discovery Studio Client software to study the binding activity of CYP51 to FLZ. (A) Molecular docking 3D diagram of FLZ and CYP51. (B) Molecular docking 2D diagram of FLZ and CYP51. The colonic contents were extracted from mice and then incubated with FLZ and Itraconazole or Voriconazole for 6 h. (C) The activity of CYP51 in gut microbiota. (D) The ratio of M1/FLZ in gut microbiota. Data are presented as mean ± SD ($n = 4$ in each group). $^{*}P < 0.05$, $^{**}P < 0.01$, $^{***}P < 0.001$ *vs.* Control.

The conversion ratio of FLZ/M1 reached its peak at 2 h (Fig. 4F), suggesting a possible conversion mode from M1 to FLZ *in vivo*. We then investigated the concentration of FLZ in the brain of mice. The results show that whether oral administration of FLZ or M1, FLZ could be detected in the brain, while the concentration of M1 was below the detection limit (0.1 ng/mL) analyzed by LC−MS/MS. It was worth noting that 2 h after administration of M1, the level of FLZ in the brain reached its peak, with the concentration-time curve consistent with that of plasma (Fig. 4G and H). These data suggest that a conversion from M1 to FLZ might exist after M1 was absorbed *in vivo.*

3.5. COMT was involved in the conversion of M1 to FLZ in blood

To confirm the conversion of M1 to FLZ after its absorption, we incubated FLZ and M1 with the mouse blood, respectively. The results showed that almost no FLZ converted to M1 in the blood (Fig. 5A), while M1 could be converted to FLZ, with a ratio of about 30% in the blood (Fig. 5B), demonstrating that M1 was remethylated in blood. Then we sought to find out which enzyme was responsible for the methylation of M1 in the blood. As COMT is the major methylase in the blood, we performed computer-assistant virtual docking by BIOVIA Discovery Studio Client software to investigate the binding activity of COMT to M1. The results show that M1 exhibited excellent docking performance on COMT with a binding free energy of −44.5554 kcal/mol (Fig. 5C and D). M1 could possibly anchor into the binding site of COMT with the following interactions: the hydrogen bond between the phenolic hydroxyl group and the site of Asp151, Ser122, Ser169; the pi−donor hydrogen bond between the benzene ring and Trp193; and the pi−anion interaction between the benzene ring and Asp151.

We employed entacapone, an inhibitor of COMT to further clarify that COMT might be a key enzyme to methylate M1. The results indicate that entacapone dose-dependently inhibited the activity of COMT in mouse blood (Fig. 5E), which accordingly, resulted in reduced concentration of FLZ and increased concentration of M1 in the blood (Supporting Information Fig. S3). And therefore, M1/FLZ ratio was reduced in the blood accordingly (Fig. 5F), suggesting that COMT might be the key enzyme in the conversion of M1 to FLZ.

3.6. Intestinal dysbacteriosis reduced FLZ absorption in the chronic PD mouse model

To further validate gut microbiota contributed to the absorption of FLZ, we developed pseudo-germ-free (PGF) mice and PGF plus MPTP/p-intoxicated PD mouse model. At the first 3 days, antibiotics were given twice a day and the colonic contents of the mice were collected on the third day for bacterial examination. The data show that oral treatment with the antibiotics for 3 days

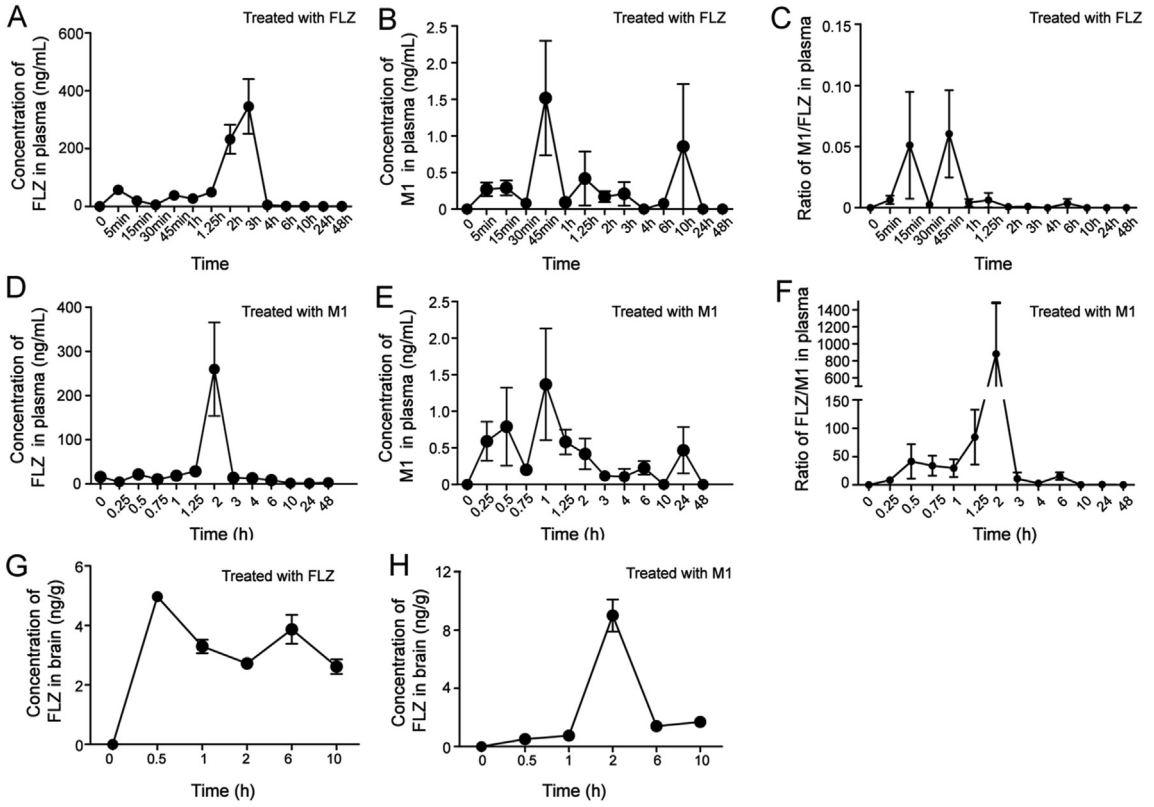

Figure 4 Pharmacokinetics study of FLZ and M1 in mice. Mice were orally administrated with FLZ (50 mg/kg) or M1 (50 mg/kg), and then plasma and brain were collected at different time points. The concentration−time curve of FLZ (A) or M1 (B) in plasma treated with FLZ. (C) The ratio of M1/FLZ in plasma treated with FLZ. The concentration−time curve of FLZ (D) or M1 (E) in plasma treated with M1. (F) The ratio of FLZ/M1 in plasma treated with M1. The concentration-time curve of FLZ in the brain treated with FLZ (G) or M1 (H). Data are presented as mean ± SD (n = 5 in each group).

reduced the bacterial colony in the mouse feces by 2 logs, indicating PGF status was developed (Supporting Information Fig. S4). Mice were then orally administrated with FLZ (75 mg/kg) for 8 weeks, meanwhile antibiotic-exposed normal control mice and MPTP/p mice were daily administrated with antibiotics for maintaining a PGF status. The results show that, compared with normal mice, the relative abundance of *Lachnospiraceae_FCS020_group*, *Bifidobacterium*, *Lactobacillus*, *Enterorhabdus*, *Tyzzerella_3*, *Bilophila*, *Eubacterium_nodatum_group*, *Anaeroplasma* significantly changed in the feces of the MPTP/p-induced PD mice (Supporting Information Table S1 and Fig. S5), while the concentrations of FLZ in PD mice were not significantly changed (Fig. 6). Then CYP51 activity was detected by microbial-derived ELISA kits assay and the result showed that CYP51 activity of PD mice was not affected compared with normal mice (Supporting Information Fig. S6), further demonstrating that the conversion of FLZ to M1 in the gut microbiota was mainly mediated by CYP51 in the gut microbiota. Fig. 6A and D shows that the concentrations of FLZ and M1 in plasma were markedly decreased in antibiotic-exposed PGF mice and PGF plus MPTP/p mice compared with their corresponding control mice, respectively. The distributions of FLZ and M1 in the brain were also markedly decreased in the PGF status of mice (Fig. 6B and E). In addition, intestinal dysbacteriosis led to increased concentration of FLZ and reduced M1 in the collected 24-h feces (Fig. 6C and F). Taken together, these data further support that the gut microbiota plays a vital role in the pharmacokinetics of FLZ.

3.7. The therapeutic efficacy of FLZ was reduced on PD mouse model with intestinal dysbacteriosis

Since the gut microbiota plays an important role in FLZ absorption, we further explored the role of the gut microbiota in the neuroprotection of FLZ in MPTP/p-induced chronic PD mouse model. Our results showed that FLZ (75 mg/kg) treatment markedly increased the time of PD mice staying on the rod, TH positive neuron numbers in the substantial nigra, and the concentration of DA and its metabolites in the striatum, suggesting the motor behavior and dopaminergic neuronal functions were improved by FLZ, while FLZ failed to alleviate the symptoms and pathology of PD in the state of PGF induced by antibiotics (Fig. 7A−F). Moreover, administration of antibiotics attenuated the inhibition of FLZ on microglia and astrocytes activation, as indicated by increased CD68 and GFAP expression, markers of microglia and astrocytes activation, compared with FLZ-treated alone in the midbrain of mice (Fig. 7G−I). Accordingly, intestinal dysbacteriosis increased mRNA expression of pro-inflammatory cytokines *Il-6*, *Il-1β*, *Iba-1*, and *Cox-2*, as well as decreased mRNA expression of anti-inflammatory cytokine *Il-10* in the midbrains of mice treated with FLZ, which were consistent with the activation of microglia and astrocytes (Fig. 7J−N). These

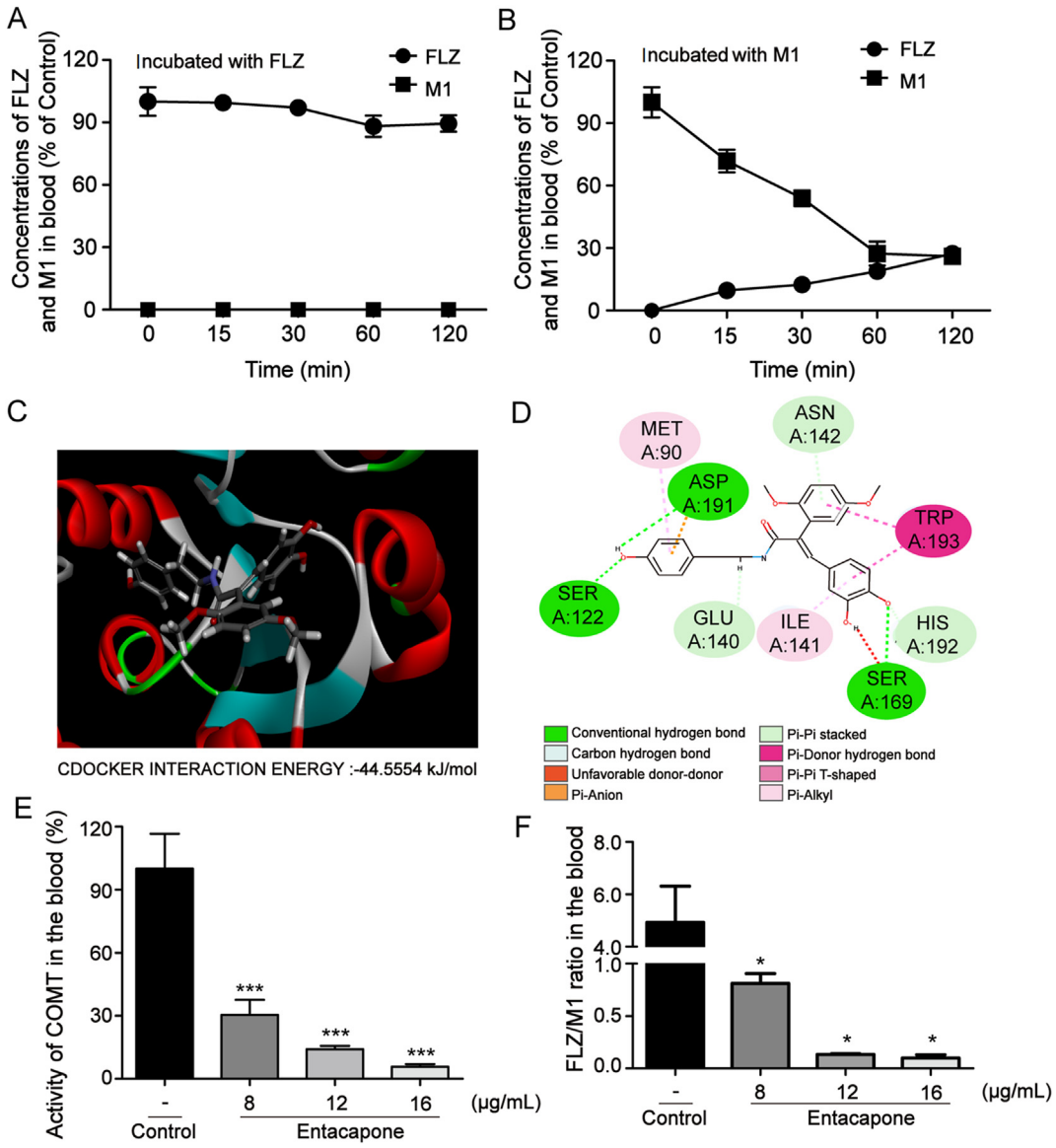

Figure 5 COMT contributed to the conversion of M1 to FLZ in the blood. Blood was collected from mice and then incubated with FLZ or M1 for 120 min. (A) Incubation of FLZ with mouse blood. (B) Incubation of M1 with mouse blood. BIOVIA Discovery Studio Client software was used to perform molecular docking of M1 and COMT. (C) Molecular docking 3D diagram. (D) Molecular docking 2D diagram. Mice blood were extracted from mice and then incubated with M1 and entacapone for 120 min: (E) The activity of COMT in the blood. (F) The ratio of FLZ/M1 in the blood. Data are presented as mean ± SD ($n = 4$ in each group). $^{**}P < 0.01$, $^{***}P < 0.001$ *vs.* Control.

results strongly suggest that the gut microbiota is a key regulator in the absorption and the following neuroprotection of FLZ on PD.

4. Discussion

In this study, we mainly investigated the critical role of gut microbiota in the absorption and efficacy of FLZ on PD, and have addressed three important findings. Firstly, M1 was the main metabolite of FLZ, which was demethylated in the gut microbiota possibly by CYP51. Secondly, M1 was then absorbed into the blood and remethylated to FLZ, which was possibly mediated by COMT. Most importantly, the disturbance of the gut microbiota induced by antibiotics decreased the absorption of FLZ, resulting in a significantly reduced level of FLZ in the blood and brain, and thereby alleviated the therapeutic efficacy of FLZ on the chronic PD mouse model. Therefore, the present study provides a paradigm showing the importance of the gut microbiota in modifying the bioavailability and therapeutic efficacy of FLZ.

Increasing evidences have been rapidly emerging that gut microbiota expresses a variety of enzymes, which could alter the activity and absorption of drugs by modifying their chemical structures[23]. It was reported that more than 30 commonly prescribed drugs were metabolically altered by the enzymes in gut microbiota[24–26], including methylase/demethylase, β-glucuronidase, nitroreductase, azoreductase, and so on[27–31]. For example, sulfasalazine, a sulfa drug used for the treatment of ulcerative colitis, is absorbed in the colon and converted to its pharmacologically active form of 5-amino 5-salicylic acid by azoreductase in gut microbiota[32,33]. FLZ is a novel synthetic derivative of squamosamide for the treatment of PD. Since its main metabolite

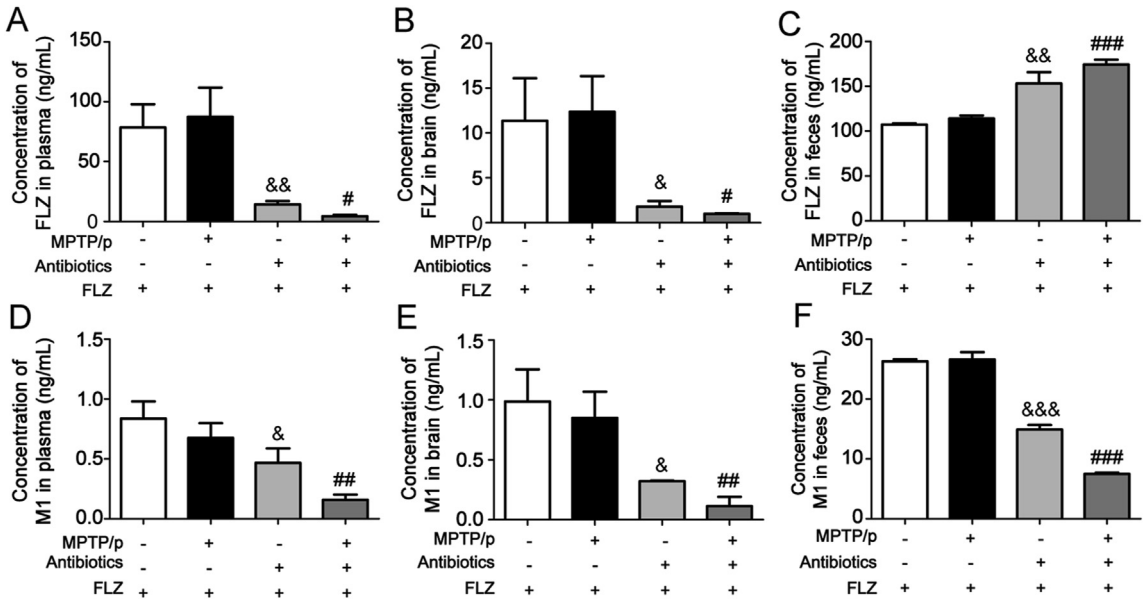

Figure 6 Effects of the gut microbiota on FLZ absorption in the chronic PD mouse model. The normal control mice, antibiotic-exposed control mice, non-antibiotic-exposed MPTP/p mice, and antibiotic-exposed MPTP/p mice were orally administrated with FLZ 75 mg/kg and the concentrations of FLZ and M1 were detected in plasma, brain, and feces by LC−MS/MS. The concentration of FLZ in the plasma (A), brain (B), and feces (C). The concentration of M1 in the plasma (D), brain (E), and feces (F). Data are presented as mean ± SD ($n = 5$ in each group). $^{\&}P < 0.05$, $^{\&\&}P < 0.01$, $^{\&\&\&}P < 0.001$ *vs*. FLZ treated Control mice; $^{\#}P < 0.05$, $^{\#\#}P < 0.01$, $^{\#\#\#}P < 0.001$ *vs*. FLZ treated antibiotic-exposed MPTP/p PD mice.

M1 almost detected in feces, we assumed gut microbiota might confer to the metabolism of FLZ. In the present study, we found that the majority of FLZ was demethylated to M1 after FLZ incubated with colonic contents, and then M1 was soon absorbed into the blood, where M1 was remethylated to FLZ. This phenomenon demonstrated that in addition to FLZ that directly absorbed into the blood, we cannot exclude that gut microbiota contributed to the absorption of FLZ.

CYP51 is a cytochrome P450 heme thiolate-containing enzyme involved in the biosynthesis of membrane sterols in all organisms from bacteria to animals[34,35]. As an important demethylase in gut microbiota, CYP51 has the characteristic of binding with palmatine, tetrahydropalmatine, dauricine, and tetrandrine, suggesting its important role in drug metabolism of gut microbiota[36–38]. After liver, kidney, and small intestine were excluded in the metabolism of FLZ to M1, we focus on CYP51 in gut microbiota in FLZ metabolism. The data show that not only high activity of CYP51 was detected in *A. baumanii*, a bacterium that could metabolize FLZ to M1, but also FLZ and CYP51 had high binding activity in virtual docking analysis, suggesting that CYP51 might mediate the demethylation of FLZ to M1. This conclusion is further supported by the fact that inhibition of CYP51 markedly reduced the FLZ-to-M1 conversion in colonic contents. Meanwhile, we found an interesting phenomenon that the concentration of FLZ in blood and brain was much higher than M1 after oral administration of M1 to mice, suggesting that there might be a pathway that remethylated M1 to its prototype FLZ. COMT is an important methylase that could catalyze the transfer of a methyl group from *S*-adenosylmethionine to drugs *in vivo*[39,40]. COMT was validated as the key enzyme that remethylated M1 to FLZ in blood, as the conversion of M1 to FLZ was markedly reduced when COMT was inhibited by entacapone. In the present study, we proposed a cyclic process for FLZ−M1−FLZ conversion, which might be one of the important mechanisms for FLZ absorption, and gut microbiota might be one of the most significant pathways involved in the pharmacokinetics of FLZ. Although CYP51 is abundant in liver as well, nearly no M1 was detected in the liver after incubating with FLZ, indicating that liver is not the main organ that metabolizes FLZ to M1. For this phenomenon, we speculated that the generated M1 from FLZ by CYP51 in liver might rapidly be converted into other metabolites by hepatic enzymes, resulting in the low concentration of M1 in liver. However, the inference needs further investigation.

Since FLZ is a potent neuroprotective agent for the treatment of PD, we further verify the role of the gut microbiota in the absorption and the therapeutic effects of FLZ on PD in a chronic mouse model induced by MPTP plus probenecid[41]. FLZ could obviously alleviate motor deficits and improve dopaminergic neuron functions, which might be due to the inhibitory effects of FLZ on neuroinflammation. To observe the role of the gut microbiota in FLZ absorption and therapeutical efficacy on PD, we treated PD mice with antibiotic cocktails to develop the PGF animal model. It is a common animal model to investigate the metabolic interaction between the host and the gut microbiota on drug biotransformation[37,41]. In this model, the antibiotic cocktail, including cefadroxil, terramycin, and erythromycin, could significantly reduce the number of the gut microbiota, and the disturbance of the gut microbiota could be considered as PFG status. In the status of the gut microbiota disturbance, the absorption of FLZ and the FLZ distribution in the brain markedly decreased, and the amount of FLZ in feces was significantly increased, which further validated that the gut microbiota was critical in the process of FLZ absorption. However, we found that compared with normal mice, although intestinal dysbacteriosis occurred in MPTP/p induced PD mouse model, the absorption of FLZ in PD mice was not decreased. We therefore designed experiment to compare the

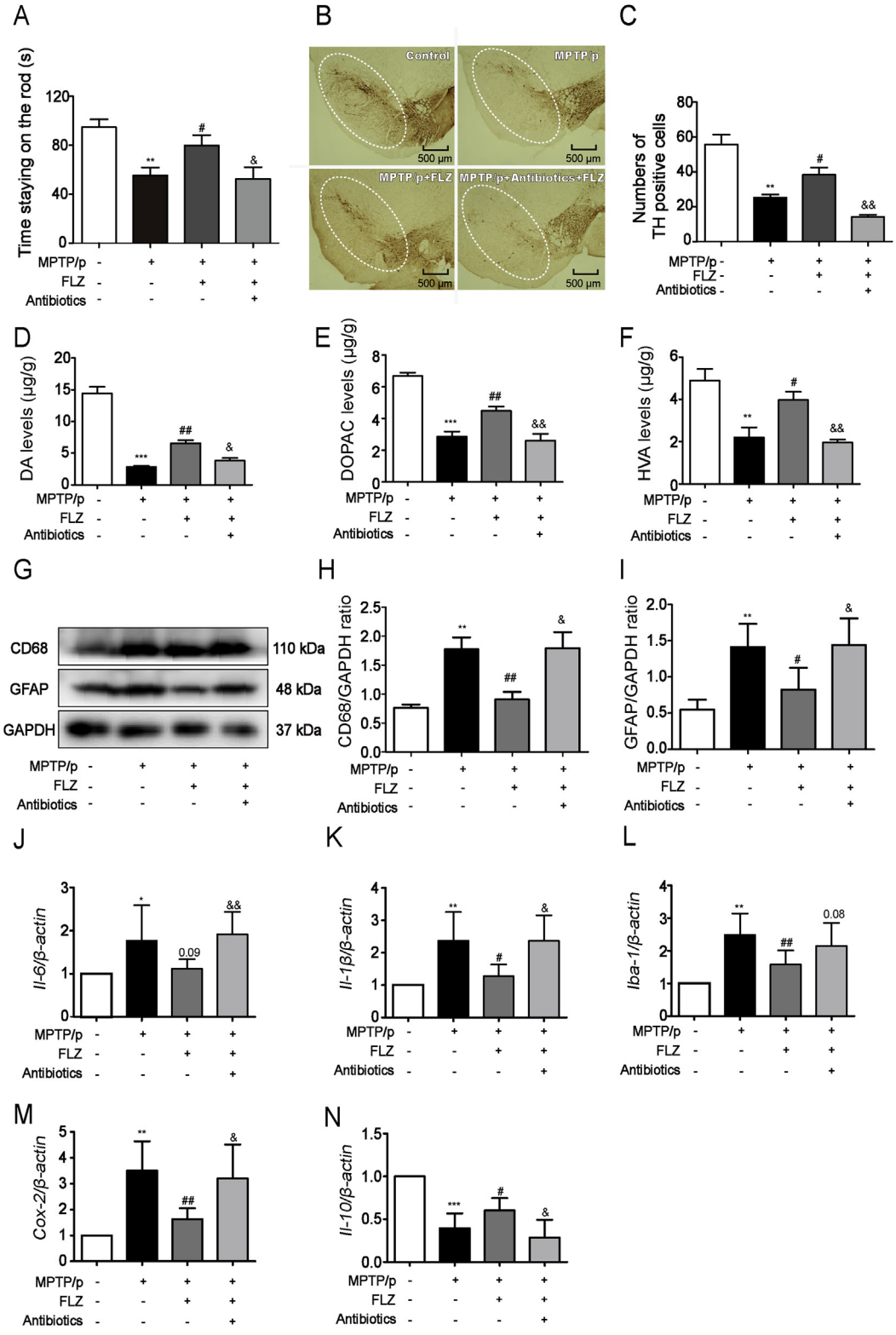

Figure 7 Effects of the gut microbiota on the neuroprotection of FLZ in MPTP/p-induced PD mouse model. FLZ (75 mg/kg) was administered to non-antibiotic-exposed MPTP/p mice and antibiotic-exposed MPTP/p mice for 8 weeks. (A) Rotarod test ($n = 12$ in each group). (B) Immunohistochemistry of TH staining in substantia nigra ($n = 4$ in each group). Representative sections of the substantia nigra from four mice were showed. (C) Numbers of TH positive cells ($n = 4$ in each group). Levels of DA (D), DOPAC (E), and HVA (F) in the striatum. (G) Representative Western blots of CD68 and GFAP. Western blot assay of CD68 (H) and GFAP (I) expression in midbrain. The mRNA expression ($n = 5$ in each group) of *Il-6* (J), *Il-1β* (K), *Iba-1* (L), *Cox-2* (M), and *Il-10* (N). Data are presented as mean ± SD. $^{*}P < 0.05$, $^{**}P < 0.01$, $^{***}P < 0.001$ *vs.* Control mice; $^{\#}P < 0.05$, $^{\#\#}P < 0.01$ *vs.* MPTP/p mice; $^{\&}P < 0.05$, $^{\&\&}P < 0.01$ *vs.* FLZ treated MPTP/p mice.

CYP51 activity in control and the chronic PD model, and verified CYP51 activity was not decreased in PD model, which might be a main reason to explain the above phenomenon. Drug stability and intact drug absorption are relevant to its pharmacological efficacy. We further investigated the role of the gut microbiota in therapeutic effects of FLZ in MPTP/p-induced PD. The results clearly show that disturbance of the gut microbiota markedly attenuated the neuroprotective effects of FLZ on PD, as demonstrated by aggravated motor behavior, reduced dopaminergic neuron functions and activated neuroinflammation. From these data, we conclude that the therapeutical effects of FLZ on PD are closely related to the gut microbiota. For one reason, the gut microbiota conferred to FLZ absorption and thus improved its efficacy, and for the other, we speculated that FLZ might directly interact with the gut microbiota and improve its efficacy through the gut−brain axis. However, the latter needs to be further elucidated.

Our findings clarify the critical roles of the gut microbiota in the metabolism and absorption of FLZ and provide a theoretical basis for the clinical pharmacokinetic studies of FLZ in the treatment of PD. In addition, the study raises an important issue for patients orally receiving FLZ treatment together with antibiotics, which contributes to the clinical rational application of FLZ. The study also suggests that the investigation of drug metabolism by the gut microbiota would be an improvement in drug development and provided new opportunities for the development of more effective or safer therapies using host-microbe combinations.

Acknowledgments

This work was supported by grants from National Sciences Foundation of China (81773718, 81630097, and 81773589), The National Key Research and Development Program of China (Grant No. SQ2018YFA090025-04), CAMS Innovation Fund for Medical Sciences (No. 2016-I2M-3-011, China), The Drug Innovation Major Project (2018ZX09711001-003-020, 2018ZX09711001-003-005, and 2018ZX09711001-008-005, China), CAMS The Fundamental Research Funds for the Central Universities (2018RC350002, China).

Author contributions

Dan Zhang, Yan Wang, and Xiuqi Bao designed the research and revised the manuscript. Junmei Shang, Shurong Ma and Caixia Zang conducted experiments, performed data analysis and contributed to the writing of the manuscript. All authors have read and approved the final manuscript.

Conflicts of interest

The authors claim that the researchers in this study have no conflict of interest.

Appendix A. Supporting information

Supporting data to this article can be found online at https://doi.org/10.1016/j.apsb.2021.01.009.

References

1. Zhao L, Shen J. Whole-body systems approaches for gut microbiota-targeted, preventive healthcare. *J Biotechnol* 2010;**149**:183−90.
2. Holmes E, Kinross J, Gibson GR, Burcelin R, Jia W, Pettersson S, et al. Therapeutic modulation of microbiota−host metabolic interactions. *Metabolism* 2018;**4**:137rv136.
3. Li Z, Quan G, Jiang X, Yang Y, Ding X, Zhang D, et al. Effects of metabolites derived from gut microbiota and hosts on pathogens. *Front Cell Infect Microbiol* 2018;**8**:314.
4. Ghaisas S, Maher J, Kanthasamy A. Gut microbiome in health and disease: linking the microbiome−gut−brain axis and environmental factors in the pathogenesis of systemic and neurodegenerative diseases. *Pharmacol Ther* 2016;**158**:52−62.
5. Tang WH, Kitai T, Hazen SL. Gut microbiota in cardiovascular health and disease. *Circ Res* 2017;**120**:1183−96.
6. Wiest R, Albillos A, Trauner M, Bajaj JS, Jalan R. Targeting the gut−liver axis in liver disease. *J Hepatol* 2017;**67**:1084−103.
7. Imhann F, Vich Vila A, Bonder MJ, Fu J, Gevers D, Visschedijk MC, et al. Interplay of host genetics and gut microbiota underlying the onset and clinical presentation of inflammatory bowel disease. *Gut* 2018;**67**:108−19.
8. Zimmermann M, Zimmermann-Kogadeeva M, Wegmann R, Goodman AL. Mapping human microbiome drug metabolism by gut bacteria and their genes. *Nature* 2019;**570**:462−7.
9. Seksik P, Landman C. Understanding microbiome data: a primer for clinicians. *Dig Dis* 2015;**33 Suppl 1**:11−6.
10. Ozdal T, Sela DA, Xiao J, Boyacioglu D, Chen F, Capanoglu E. The reciprocal interactions between polyphenols and gut microbiota and effects on bioaccessibility. *Nutrients* 2016;**8**:78.
11. Zhao ZX, Fu J, Ma SR, Peng R, Yu JB, Cong L, et al. Gut−brain axis metabolic pathway regulates antidepressant efficacy of albiflorin. *Theranostics* 2018;**8**:5945−59.
12. Wilson ID, Nicholson JK. Gut microbiome interactions with drug metabolism, efficacy, and toxicity. *Transl Res* 2017;**179**:204−22.
13. Zahran SA, Ali-Tammam M, Hashem AM, Aziz RK, Ali AE. Azoreductase activity of dye-decolorizing bacteria isolated from the human gut microbiota. *Sci Rep* 2019;**9**:5508.
14. Lowry PW, Franklin CL, Weaver AL, Szumlanski CL, Mays DC, Loftus EV, et al. Leucopenia resulting from a drug interaction between azathioprine or 6-mercaptopurine and mesalamine, sulphasalazine, or balsalazide. *Gut* 2001;**46**:656−64.
15. Ryan A, Wang CJ, Laurieri N, Westwood I, Sim E. Reaction mechanism of azoreductases suggests convergent evolution with quinone oxidoreductases. *Protein Cell* 2010;**1**:780−90.
16. Zhang D, Zhang JJ, Liu GT. The novel squamosamide derivative FLZ protects against 6-hydroxydopamine-induced apoptosis through inhibition of related signal transduction in SH-SY5Y cells. *Eur J Pharmacol* 2007;**561**:1−6.
17. Tai W, Ye X, Bao X, Zhao B, Wang X, Zhang D. Inhibition of Src tyrosine kinase activity by squamosamide derivative FLZ attenuates neuroinflammation in both *in vivo* and *in vitro* Parkinson's disease models. *Neuropharmacology* 2013;**75**:201−12.
18. Bao XQ, Kong XC, Qian C, Zhang D. FLZ protects dopaminergic neuron through activating protein kinase B/mammalian target of rapamycin pathway and inhibiting RTP801 expression in Parkinson's disease models. *Neuroscience* 2012;**202**:396−404.
19. Wang Y, Shou JW, Li XY, Zhao ZX, Fu J, He CY, et al. Berberine-induced bioactive metabolites of the gut microbiota improve energy metabolism. *Metabolism* 2017;**70**:72−84.
20. Bao XQ, Wang XL, Zhang D. FLZ Attenuates alpha-synuclein-induced neurotoxicity by activating heat shock protein 70. *Mol Neurobiol* 2017;**54**:349−61.
21. Li DC, Bao XQ, Wang XL, Sun H, Zhang D. A novel synthetic derivative of squamosamide FLZ inhibits the high mobility group box 1 protein-mediated neuroinflammatory responses in murine BV2

microglial cells. *Naunyn Schmiedebergs Arch Pharmacol* 2017;**390**:643−50.
22. Rabelo VW, Santos TF, Terra L, Santana MV, Castro HC, Rodrigues CR, et al. Targeting CYP51 for drug design by the contributions of molecular modeling. *Fundam Clin Pharmacol* 2017;**31**:37−53.
23. Spanogiannopoulos P, Bess EN, Carmody RN, Turnbaugh PJ. The microbial pharmacists within us: a metagenomic view of xenobiotic metabolism. *Nat Rev Microbiol* 2016;**14**:273−87.
24. Noh K, Kang YR, Nepal MR, Shakya R, Kang MJ, Kang W, et al. Impact of gut microbiota on drug metabolism: an update for safe and effective use of drugs. *Arch Pharm Res* 2017;**40**:1345−55.
25. Curro D. The role of gut microbiota in the modulation of drug action: a focus on some clinically significant issues. *Expert Rev Clin Pharmacol* 2018;**11**:171−83.
26. Wang Y, Tong Q, Shou JW, Zhao ZX, Li XY, Zhang XF, et al. Gut microbiota-mediated personalized treatment of hyperlipidemia using berberine. *Theranostics* 2017;**7**:2443−51.
27. Chen K, Luan X, Liu Q, Wang J, Chang X, Snijders AM, et al. *Drosophila* histone demethylase KDM5 regulates social behavior through immune control and gut microbiota maintenance. *Cell Host Microbe* 2019;**25**:537−552 e538.
28. Pollet RM, D'Agostino EH, Walton WG, Xu Y, Little MS, Biernat KA, et al. An Atlas of beta-glucuronidases in the human intestinal microbiome. *Structure* 2017;**25**:967−977 e965.
29. Kapetanovic IM, Lyubimov AV, Kabirova EV, Kabirov KK, Rasay L, Swezey R, et al. Effects of bacterial and presystemic nitroreductase metabolism of 2-chloro-5-nitro-*N*-phenylbenzamide on its mutagenicity and bioavailability. *Chem Biol Interact* 2012;**197**:16−22.
30. Yoon WJ, Kim HN, Park E, Ryu S, Chang Y, Shin H, et al. The impact of cholecystectomy on the gut microbiota: a case-control study. *J Clin Med* 2019;**8**:79.
31. Blanton LV, Barratt MJ, Charbonneau MR, Ahmed T, Gordon JI. Childhood undernutrition, the gut microbiota, and microbiota-directed therapeutics. *Science* 2016;**352**:1533.
32. Ryan A, Kaplan E, Nebel JC, Polycarpou E, Crescente V, Lowe E, et al. Identification of NAD(P)H quinone oxidoreductase activity in azoreductases from *P. aeruginosa*: azoreductases and NAD(P)H quinone oxidoreductases belong to the same FMN-dependent superfamily of enzymes. *PLoS One* 2014;**9**:e98551.
33. Jilani JA, Shomaf M, Alzoubi KH. Synthesis and evaluation of mutual azo prodrug of 5-aminosalicylic acid linked to 2-phenylbenzoxazole-2-yl-5-acetic acid in ulcerative colitis. *Drug Des Devel Ther* 2013;**7**:691−8.
34. Morrison AM, Goldstone JV, Lamb DC, Kubota A, Lemaire B, Stegeman JJ. Identification, modeling and ligand affinity of early deuterostome CYP51s, and functional characterization of recombinant zebrafish sterol 14alpha-demethylase. *Biochim Biophys Acta* 2014;**1840**:1825−36.
35. Matowane RG, Wieteska L, Bamal HD, Kgosiemang IKR, van Wyk M, Manume NA, et al. *In silico* analysis of cytochrome P450 monooxygenases in chronic granulomatous infectious fungus *Sporothrix schenckii*: special focus on CYP51. *Biochim Biophys Acta Proteins Proteom* 2018;**1866**:166−77.
36. He CY, Fu J, Shou JW, Zhao ZX, Ren L, Wang Y, et al. *In vitro* study of the metabolic characteristics of eight isoquinoline alkaloids from natural plants in rat gut microbiota. *Molecules* 2017;**22**:932.
37. Ekins S, de Siqueira-Neto JL, McCall LI, Sarker M, Yadav M, Ponder EL, et al. Machine learning models and pathway genome data base for trypanosoma cruzi drug discovery. *PLoS Negl Trop Dis* 2015;**9**:e0003878.
38. Hosang GM, Fisher HL, Cohen-Woods S, McGuffin P, Farmer AE. Stressful life events and catechol-*O*-methyl-transferase (*COMT*) gene in bipolar disorder. *Depress Anxiety* 2017;**34**:419−26.
39. Lee BW, Sun HG, Zang T, Kim BJ, Alfaro JF, Zhou ZS. Enzyme-catalyzed transfer of a ketone group from an *S*-adenosylmethionine analogue: a tool for the functional analysis of methyltransferases. *J Am Chem Soc* 2010;**132**:3642−3.
40. Gibrat C, Saint-Pierre M, Bousquet M, Levesque D, Rouillard C, Cicchetti F. Differences between subacute and chronic MPTP mice models: investigation of dopaminergic neuronal degeneration and alpha-synuclein inclusions. *J Neurochem* 2009;**109**:1469−82.
41. Hernández-Chirlaquea C, Arandaa CJ, Ocónb B, Capitán-Cañadasa F, Mercedes, Ortega-Gonzáleza, et al. Germ-free and antibiotic-treated mice are highly susceptible to epithelial injury in DSS colitis. *J Crohns Colitis* 2016;**10**:1324−35.